Available online at www.sciencedirect.com

ScienceDirect

Energy Procedia 111 (2017) 914 – 923

Energy Procedia

8th International Conference on Sustainability in Energy and Buildings, SEB-16, 11-13 September 2016, Turin, ITALY

Real Time Fault Detection in Photovoltaic Systems

Mohamed Hassan Ali[a,c]*, Abdelhamid Rabhi[a], Ahmed El hajjaji[a] and Giuseppe M. Tina[b]

[a]*MIS Laboratory, University of Picardie Jules Verne, 14 Quai de Somme, Amiens 80000, France*
[b]*DIEEI Departement, University of Catania, 2 Piazza Università, Catania 95124, Italy*
[c]*CRUD, University of Djibouti, Avenue Djanaleh, Djibouti BP1904, Djibouti*

Abstract:

In this paper, a method for real time monitoring and fault diagnosis in photovoltaic systems is proposed. This approach is based on a comparison between the performances of a faulty photovoltaic module, with its accurate model by quantifying the specific differential residue that will be associated with it. The electrical signature of each default will be fixed by considering the deformations induced on the I-V curves. Some faults, such as: interconnection resistance faults and different shading patterns are considered. The proposed technique can be generalized and extended to more types of faults. The fault diagnosis will be determined by fixing a normal and a fault threshold for each fault. These thresholds are calculated based on the Euclidean norm between ideal and normal measurement or between ideal and fault mode measurement. Each threshold is set in a range bounded by the minimum and maximum values of the differential residue obtained for the considered fault. The proposed approach provides identification of faults by calculating their specific threshold ranges. This method allows the instantaneous monitoring of the electrical power delivered by the photovoltaic system.

Peer-review under responsibility of KES International.

Keywords: diagnosis; electrical signature; threshold of failure; model power; modeling

1. Introduction

Solar energy is the most abundant, inexhaustible and clean of all renewable energy resources. Interest in photovoltaic power generation has increased in recent years thanks to its advantages. This wide distribution of photovoltaic panel production was not followed by monitoring, fault detection and diagnosis functions to ensure better profitability. Numerous studies have been done on diagnosis of photovoltaic systems but just a few have been reported for describing and localizing faults in PV systems. They are not directly applicable to conventional PV systems and they require a relatively high cost in equipment.

* Corresponding author. Tel.: +33 322825916; fax: +33 322825905.
E-mail address: mohamed.hassan.ali@u-picardie.fr

Peer-review under responsibility of KES International.
doi:10.1016/j.egypro.2017.03.254

Fault detection methods for photovoltaic systems are numerous (electrical characterization, visual inspection, ultrasonic inspection, infrared imaging, imaging…) [1]. Some methods use appropriate equipment (thermal camera…). These visual inspection or the thermal detection methods, require visual checking with frequent visits on the PV module to monitor changes in its appearance as indicators of failures: browning, mechanical damage or occurrence of hot spots… Electrical diagnostic methods specifically uses the electronic signature of faults. They continuously monitor the PV module performance until the appearance of a fault. The deformation of the resulting output provides information on the occurrence, location and nature of default [2]. The first indication of module degradation is provided by decrease in its output power. Resulting symptoms are presented by the I-V curves of electrical characterizations of the PV module. After detection, microscopic analysis can be performed to understand causes of the degradation. These techniques allow analysis of the induced degradation and its progression.

Nomenclature

T	Cell temperature (°C)
G	Global irradiation on the array surface (W/m^2)
STC	Standard test condition of the PV cell; T_{STC} = 25°C and G_{STC} = 1000 W/m^2
PV	Photovoltaic
q	Electron charge (1.6*10^{-19} C)
K	Boltzmann constant (1.38*10^{-23} Nm/K)
I_{PV}	Light generated current of a PV module (A)
I	PV module current (A)
V	PV module voltage (V)
I_{MPP}	Maximum power point current (A)
V_{MPP}	Maximum power point voltage (V)
I_{SC}	Short-circuit current (A)
V_{OC}	Open-circuit voltage (V)
V_{T1}	Thermodynamic voltage of diode 1 (V)
V_{T2}	Thermodynamic voltage of diode 2 (V)
a, a_1, a_2	Ideality factors of the cell
I_0 /I_{01}, I_{02}	Saturation currents of cell for 1Diode model / 2Diode model (A)
$RX_{id,ft}$	Residual signals generated from the difference between X_{id} and X_{ft}
$RX_{id,nm}$	Residual signals generated from the difference between X_{id} and X_{nm}
X_{ft}	Set of the output variables (I_{mpp}, V_{mpp}, I_{sc}, V_{oc}, S_1, S_2, S_3) in faulty condition
X_{nm}	Set of the output variables (I_{mpp}, V_{mpp}, I_{sc}, V_{oc}, S_1, S_2, S_3) in normal condition
X_{id}	Set of the output variables (I_{mpp}, V_{mpp}, I_{sc}, V_{oc}, S_1, S_2, S_3) in ideal condition
N_F	Square root of the root of $RX_{id,ft}$
N_N	Square root of the root of $RX_{id,nm}$
S_1	Incremental derivative ratio between the point (0; I_{sc}) and the point (V_{mpp}; I_{mpp}) (Ω^{-1})
S_2	Incremental derivative ratio between the point (V_{mpp}; I_{mpp}) and the point (V_{oc}; 0) (Ω^{-1})
S_3	Value of the variation of the series resistance (Ω)
R_S	Series resistance of diode model (Ω)
R_P	Parallel resistance of diode model (Ω)
T_{NOCT}	Normal operating cell temperature (°C)
K_I	Temperature coefficient of short-circuit current (%/°C)
K_V	Temperature coefficient of Open-circuit voltage (mV/°C)
ΔT	Difference between actual temperature and T_{STC} (°C)
Ns	Number of cells connected in series

First, we propose to set different specific electrical signatures to several faults. Specifically in this article, we focus on partial shading fault and interconnection resistance fault.

As following method proposed in [3], we suggest to consider six variables from three major points of each I-V curve: A (I_{MPP}, V_{MPP}), B (I_{SC}, 0), C (0, V_{OC}) and three associated parameters, S_1 defines the slope between the short-circuit point and the maximum point and S_2 the slope between the maximum and the open circuit point and then S_3 expresses variation of R_S. We will therefore be able to assess the impact of the arrival of a fault on six variables across the

observed deformation of I-V curves and associate it a signature as set in [4]. The proposed diagnosis approach will focus on the comparison between the modeled ideal power and the measured power achieved by a real time acquisition.

2. Modelling and validation of the photovoltaic panel model

Due to the importance of PV system modelling, in literature, there are different approaches to model PV systems, specifically PV modules [3, 4, 5]. The mathematical models are usually based on physical processes that occur in the system and on factors influencing these processes. The basic element in a PV system is a PV module that is made of PV cells connected in series or in parallel. The two-diode equivalent electrical model, shown in Fig. 1, represents either a single cell or a PV module according to the values of the main electrical variables (e.g. I and V) and of parameters (e.g. R_S and R_P).

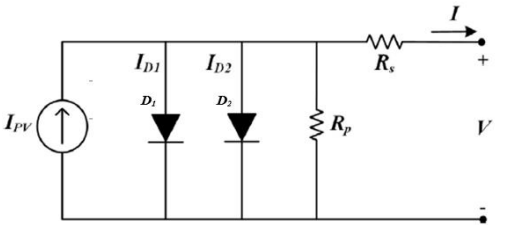

Fig. 1. Two-diode equivalent electrical circuit model for a PV cell/module

The nonlinear equation between the module current and voltage (1), has seven parameters a_1, a_2, R_S, R_P, I_{01}, I_{02} and I_{PV}.

$$I = I_{PV} - I_{01} * \left(\exp\left(\frac{V + I * R_S}{a_1 * V_{T1}} \right) - 1 \right) - I_{02} * \left(\exp\left(\frac{V + I * R_S}{a_2 * V_{T2}} \right) - 1 \right) - \frac{V + I * R_S}{R_P} \quad (1)$$

Where:
a_1 and a_2 are the diode quality factors for, respectively, D_1 and D_2;
I_{01} and I_{02} are the saturation currents for D_1 and D_2 respectively.
Some parameters in Eq. (1) depend on operating conditions such as irradiance on the surface of the module, G, and PV module temperature, T. These dependencies are reported in the following expressions [6, 7]:

$$I_{PV} = \left(I_{PV\_STC} + K_I * \Delta T \right) * \frac{G}{G_{STC}} \quad (2)$$

$$I_{01} = \left(I_{SC\_STC} + K_I * \Delta T \right) / \left(\exp\left(\left(V_{OC\_STC} + K_V * \Delta T \right) / a_1 * V_{T1} \right) - 1 \right) \quad (3)$$

$$I_{02} = \left(I_{SC\_STC} + K_I * \Delta T \right) / \left(\exp\left(\left(V_{OC\_STC} + K_V * \Delta T \right) / a_2 * V_{T2} \right) - 1 \right) \quad (4)$$

With:

$$V_{T1} = V_{T2} = N_S * K * T / q \quad \text{and} \quad \Delta T = T - T_{STC} \quad (5)$$

In (2) to (4), the variables and parameters with the STC notation indicate that they have been measured/evaluated at Standard Test Conditions (STC measurement conditions: G_{STC}=1000 W/m², AM 1.5; T_{STC}= 25°C). K_I and K_V are the thermal coefficients, respectively of the short circuit current and of the open circuit voltage, such values are provided by the manufacturer of the PV module (see Table 1). Without any meaningful effects on accuracy, the two-diode model can be simplified by neglecting the series resistance (R_S =0). This decreases the number of parameters from seven to six: a_1, a_2, I_{01}, I_{02}, I_{PV}, R_P. As a result of this [8], we have:

$$I = I_{PV} - I_{01} * \left(\exp\left(\frac{V}{a_1 * V_{T1}} \right) - 1 \right) - I_{02} * \left(\exp\left(\frac{V}{a_2 * V_{T2}} \right) - 1 \right) - \frac{V}{R_P} \quad (6)$$

In Table 1 the characteristic data of the PV module used to acquire the experimental data in the present paper, are reported in [9].

Table 1. Data of p-Si panel China light Solar CLS 220P.

Model China Light Solar CLS 220P	Electrical Data
Nominal power P_{MAX} [W]	220
Maximum voltage V_{MPP} [V]	28.9
Maximum current I_{MPP} [A]	7.61
Open circuit voltage Voc [V]	36.8
Open circuit current Isc [A]	8.24
Minimum power guarantied P_{MIN} [W]	220
Output efficiency [%]	13.5
Maximum voltage of system [V_{DC}]	1000
Temperature factor of P_N [%/°C]	-0.0044
Temperature factor of V_{DC} [V/°C]	-0.0032
Temperature factor of Isc [mA/°C]	0.0004
T_{NOCT} [°C]	47
Number of cells	60

In order to extract PV parameters, several researches exist in literature about the calculation of these parameters to build the mathematical model of the PV module. The most known techniques are based on iterative mathematical calculation.

In this paper, we perform parameters extraction by using Particle Swarm Optimization algorithm (PSO).The Particle Swarm Optimization algorithm is inspired by the swarm intelligence of bird flocking [10]. It is initialized with a population of random solutions, particles, within a predefined solution.

At each iteration, the position and velocity of each particle are adjusted in light of the personal best experience of the particle and that of the entire swarm. The weights of the two factors are determined by a system of randomized correction coefficients. As the particles converge toward the optimal solution an inertia weight parameter is used to maintain the balance between global and local search capability of the algorithm.

In literature, some authors developed applications with this method adapted to PV system. The extracted parameters have been studied to identify the different mechanisms affecting PV performance as seen in [11].

The main approach proposed and used here which is "Fractional Order Darwinian Particle Swarm Optimization" (FODPSO), improves performances of the PSO method and adapts them to obtain exact results and appropriate representations from real measurements.

To adapt the response of the used Simulink model to a particular temperature and illumination point, we applied the following equations, (7) to (11) from literature, to determine the three major points of the I-V curves, i.e. (I_{SC}; 0), (I_{MPP};V_{MPP}), (0;V_{OC}) [12, 13]:

$$V_{OC} = V_{OC\_STC} + \left(K_V * \Delta T\right) \tag{7}$$

$$I_{SC} = I_{SC\_STC} * \frac{G}{G_{STC}} * \left(1 + K_I * \Delta T\right) \tag{8}$$

$$I_{PV\_STC} \approx I_{SC\_STC} \tag{9}$$

$$I_{MPP} = I_{MPP\_STC} * \frac{G}{G_{STC}} \tag{10}$$

$$V_{MPP} = V_{MPP\_STC} + \left(K_V * \Delta T\right) \tag{11}$$

To validate our approach, we used real data from the platform. The experimental photovoltaic generator used in this study is a string formed by three Polycrystalline PV modules, CLS-220P by CHINALIGHT Solar Co, connected in series. Each module contains 60 series connected PV cells gathered into three sub-strings, each one is constituted by 20 PV cells and connected in anti-parallel with a bypass diode. The experimental setup (PV string; electronic load and

acquisition system) is installed in the power system laboratory at the DIEEI Department of University of Catania (Italy), as it is shown in Fig. 2.

Fig. 2. Renewable energy platform in Catania University-

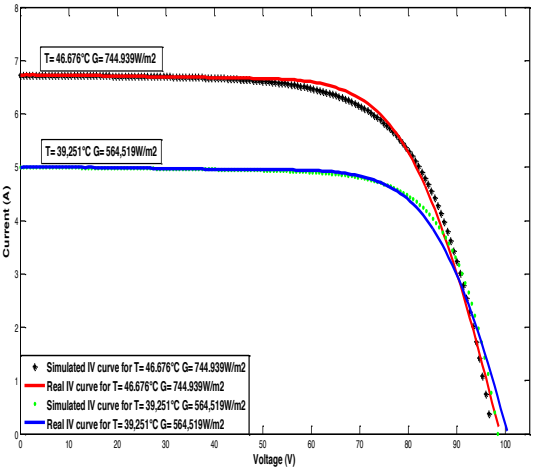

Fig. 3. Measured and simulated I-V curves under different measured incident irradiance (G) and PV cells temperature (T).

The set of curves presented in figure 3, complies with the specifications provided by the measured and simulated characteristics and thereafter the values of the six main parameters (a_1, a_2, I_{01}, I_{02}, I_{PV}, R_P) for 2D model with R_S neglected.

3. Proposed method for monitoring and fault detection

The diagnosis enables detection, isolation and identification of a fault that reached a critical threshold. Detection of this fault consists of indicating whether a failure appears on the concerned system. The isolation of a failure is meant for locating the failed component and then comes the identification of its nature [14]. Overall, this is to compare in faulty condition threshold with system operation in nominal condition. There are many approaches and the choice of one technique depends on:

- knowledge of the history of system events
- the expert system knowledge
- data collected on the system in normal operation conditions
- a known model of the system

As a result, we can summarize a classification of the most common diagnosis methods as reported in Fig.4.

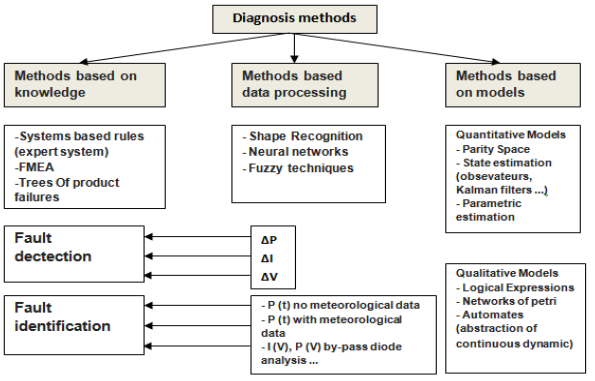

Fig. 4. Diagnosis methods

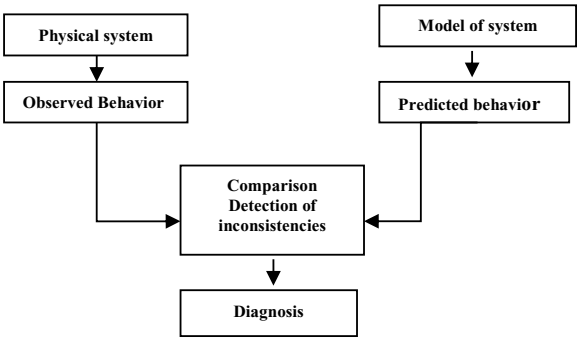

Fig. 5. Model-based diagnosis

In this study, we focus in particular on model-based diagnosis defined in Fig.5. The method of diagnosis presented in this paper, consists of two parts, passive and active. Both parts act in sequence to a constant scanning of the instantaneous power delivered by the module for real-time monitoring [15].

3.1. Passive part of diagnosis

The passive part of diagnosis involves comparing in real time the measured power and that obtained by the model. The majority of degradations of known PV modules directly influence the power losses [14] [16]. Our diagnosis strategy is to control and to observe produced power. In this regards, we measure voltage and current in real time and calculate the produced power by PV system. This captured data is compared with the simulation results. The fault detection will be determined by fixing a normal threshold and a failure threshold. In this section, each value of residue is generated using the diagnosis method based on the model. We use the model developed in the previous paragraph.

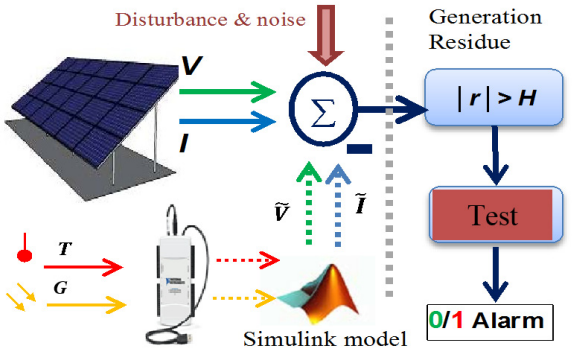

Fig. 6. Structure of first part of diagnosis system

This model has the following advantages:
- Applicable to almost all commercial PV panels.
- Capable to work in real-time for fault diagnosis deliberation and monitoring system.
- Capable to simulate partial shading (PSC) effect and degradation to investigate panel fault.
- Can be easily connected and interfaced with the electronic devices and power converter models in Matlab Simulink for maximum power point tracking studies.

The residual signal is generated in real time by comparing real measured power and the simulation results on Matlab. For fault detection, a simple solution is to compare the level of residue in a predefined threshold beyond which the presence of a fault is confirmed.

There is an important variety of faults which can modify the instantaneous power of a photovoltaic module. Shading is one of the most recurrent and damageable faults [17] along with resistive faults on the interconnection between substrings in the same module or between modules. In our study, we present five scenarios of different faults:

- Fault 1: Condition where a third part of module 1 and 2 is shaded only (case A),
- Fault 2: Condition where 3 cells per module of each module are shaded (case B),
- Fault 3: Condition where half part of each module are shaded (case C),
- Fault 4: a line resistance connected having value R_C=3Ω which represent resistive losses on connections.
- Fault 5: a line resistance connected having value R_C=5Ω which represent resistive losses on connections.

3.2. Active part of diagnosis

When an unquestionably alarm signal is appeared from the passive part of test, fault detection algorithm is interrupted and it jumps to active part of test procedure. This test must be done very fast to record accurate and precise data. The rates of change for irradiation is well-nigh 200 W. $m^{-2}.s^{-1}$ under partly cloudy conditions according to IEC 61724 international standard. To meet standard condition, the flash test time must be less than 50ms. Flash test is a

fundamental method for measuring the I-V characteristics of photovoltaic panels by spanning the PV voltage from zero to open circuit in a short time [18].

This method is to diagnose five kinds of faults in real time by comparing the residuals between ideal modelled power and measured power in normal condition on one hand and between ideal power and fault condition measured power on the other hand. After that, we can test these residues with the calculated normal threshold by using Euclidean distance method. To illustrate the proposed method of diagnosis, we measured separately the instantaneous power produced by the photovoltaic system formed with three modules in series in normal and faulty conditions for each of the five considered faults (Fig.7). The ideal condition values are provided to us by Simulink model without uncertainties of measurements on field in order to calculate both thresholds of normality and fault in each cases.

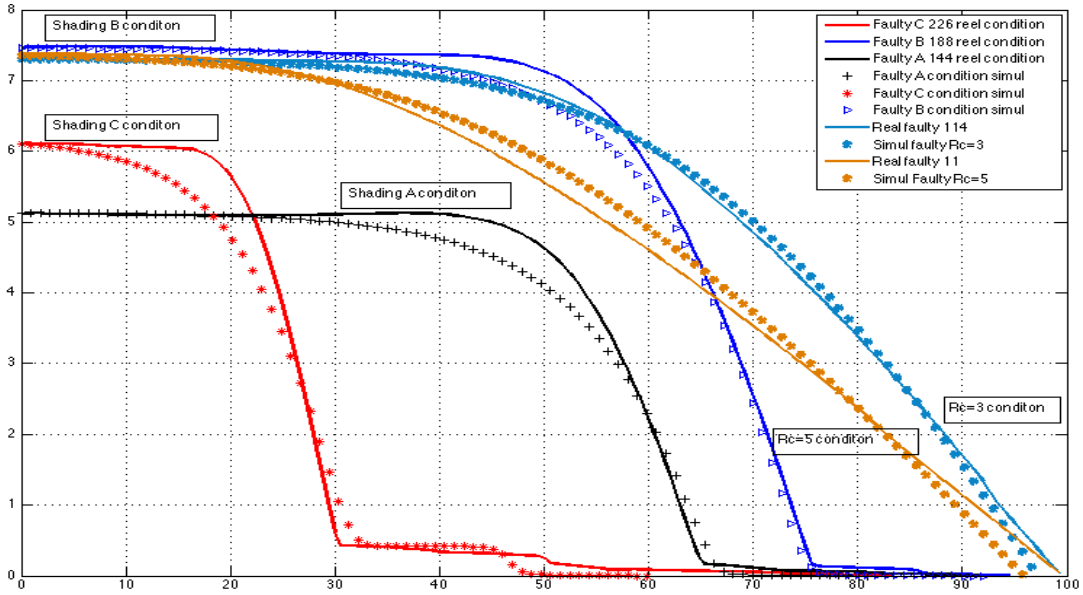

Fig. 7. Measured and simulated I-V curves for 2 different cases of connection faults and 3 different partial shading conditions

Afterwards, we calculate the thresholds for normality and for each fault by the two following methods:

$$|N_N| = \sqrt{\sum_{i=1}^{6} \left(RX_{id,nm}\right)^2} \quad RX_{id,nm} = X_{id} - X_{nm} \quad (12) \qquad |N_F| = \sqrt{\sum_{i=1}^{6} \left(RX_{id,ft}\right)^2} \quad RX_{id,ft} = X_{id} - X_{ft} \quad (13)$$

The electrical signature of faults is defined by the deformation observed in the curves. That is why we considered six particular quantities: the three main points of short circuit, open circuit and maximum operating point (I_{SC}; V_{OC}; I_{MPP}; V_{MPP}) on one hand and three associated values S_1, S_2, S_3 on the other hand. The associated values S_1, S_2 reflect the deformations of the slopes of the two parts of the IV curves whereas S_3 relates to variations in R_S. For each default, we obtained the following values, which reflect the curves in failure mode, ideal and normal (Table 2 to Table 6).

Table 2. Calculation of the seven parameters for ideal, normal and faulty mode for Shading A.

Parameters	Ideal condition	Normal condition	Abnormal condition
I_{SC} [A]	5.139	5.126	5.116
I_{MPP} [A]	4.392	4.771	4.692
V_{MPP} [V]	76.38	74.25	49.4
V_{OC} [V]	97.55	99.44	65.26
$S_1=(I_{MPP}-I_{SC})/(V_{MPP}-V_{OC})[\Omega^{-1}]$	0.0352	0.0141	0.0267
$S_2=(0-I_{MPP})/(V_{OC}-V_{MPP})[\Omega^{-1}]$	-0.2075	-0.1894	-0.2958
$S_3=\Delta R_S=\Delta V_{MPP}/\Delta I_{MPP}[\Omega]$	$1e^{-5}$	0.485	6.143

Table 3. Calculation of the seven parameters for ideal, normal and faulty mode for Shading B.

Parameters	Ideal condition	Normal condition	Abnormal condition
I_{SC} [A]	7.471	7.491	7.466
I_{MPP} [A]	6.389	6.84	7.017
V_{MPP} [V]	76.86	70.67	51.64
V_{OC} [V]	95.71	98.15	76.2
$S_1=(I_{MPP}-I_{SC})/(V_{MPP}-V_{OC})[\Omega^{-1}]$	0.0574	0.0237	0.0183
$S_2=(0-I_{MPP})/(V_{OC}-V_{MPP})[\Omega^{-1}]$	-0.3389	-0.2489	-0.2857
$S_3=\Delta R_S=\Delta V_{MPP}/\Delta I_{MPP}[\Omega]$	$1e^{-5}$	0.9689	3.9474

Table 4. Calculation of the seven parameters for ideal, normal and faulty mode for Shading C.

Parameters	Ideal condition	Normal condition	Abnormal condition
I_{SC} [A]	6.178	6.078	6.109
I_{MPP} [A]	5.269	5.469	5.754
V_{MPP} [V]	76.38	73.65	19.45
V_{OC} [V]	96.7	98.16	31.11
$S_1=(I_{MPP}-I_{SC})/(V_{MPP}-V_{OC})[\Omega^{-1}]$	0.0447	0.0252	0.0304
$S_2=(0-I_{MPP})/(V_{OC}-V_{MPP})[\Omega^{-1}]$	-0.2593	-0.2259	-0.4935
$S_3=\Delta R_S=\Delta V_{MPP}/\Delta I_{MPP}[\Omega]$	$1e^{-5}$	0.4612	10.8047

Table 5. Calculation of the seven parameters for ideal, normal and faulty mode for Rc=3Ω.

Parameters	Ideal condition	Normal condition	Abnormal condition
I_{SC} [A]	7.316	7.328	7.306
I_{MPP} [A]	6.444	6.451	6.771
V_{MPP} [V]	73.62	73.55	50.95
V_{OC} [V]	95.71	98.51	99.26
$S_1=(I_{MPP}-I_{SC})/(V_{MPP}-V_{OC})[\Omega^{-1}]$	0.0395	0.0351	0.0111
$S_2=(0-I_{MPP})/(V_{OC}-V_{MPP})[\Omega^{-1}]$	-0.2917	-0.2585	-0.1402
$S_3=\Delta R_S=\Delta V_{MPP}/\Delta I_{MPP}[\Omega]$	$1e^{-5}$	0.0109	3.5180

Table 6. Calculation of the seven parameters for ideal, normal and faulty mode for Rc=5Ω.

Parameters	Ideal condition	Normal condition	Abnormal condition
I_{SC} [A]	7.395	7.396	7.363
I_{MPP} [A]	6.406	6.811	6.869
V_{MPP} [V]	74.54	68.99	31.73
V_{OC} [V]	95.71	97.63	99.17
$S_1=(I_{MPP}-I_{SC})/(V_{MPP}-V_{OC})[\Omega^{-1}]$	0.0467	0.0204	0.0073
$S_2=(0-I_{MPP})/(V_{OC}-V_{MPP})[\Omega^{-1}]$	-0.3026	-0.2378	-0.1019
$S_3=\Delta R_S=\Delta V_{MPP}/\Delta I_{MPP}[\Omega]$	$1e^{-5}$	0.8664	6.6828

These five tables at particular points allow us to determine the normal and faulty thresholds for each considered fault by Euclidean distance (Table 7). Determination of seven parameters allows to know the induced deformation for each fault.

Table 7. Normal threshold and Faulty threshold for each kind of default by EC method.

Residues	N_N	N_F
Fault 1	2.9136	42.5253
Fault 2	6.7395	32.1352
Fault 3	2.8811	87.5221
Fault 4	2.8011	23.2172
Fault 5	5.9505	43.4694

Then, we can apply different thresholds to the ideal instantaneous power and the faulty instantaneous power. Corresponding residue is compared with calculated thresholds for each fault. A Boolean response is obtained for the diagnosis of the five-targeted faults. Subsequently, we obtained the following results by the Euclidean distance for each studied case. We succeeded to detect the five different faults. The results can be shown in figures 8 to 17.

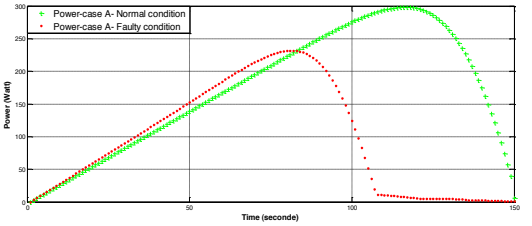

Fig. 8. Normal and faulty power for Shading A

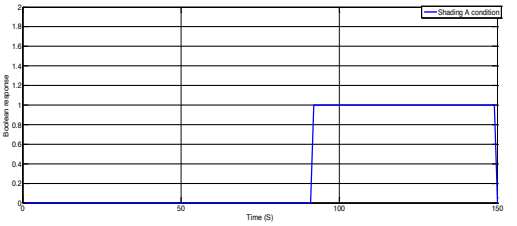

Fig. 9. Boolean response for Shading A

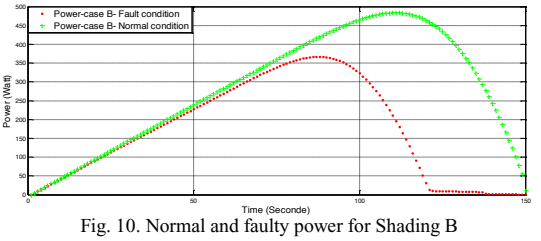

Fig. 10. Normal and faulty power for Shading B

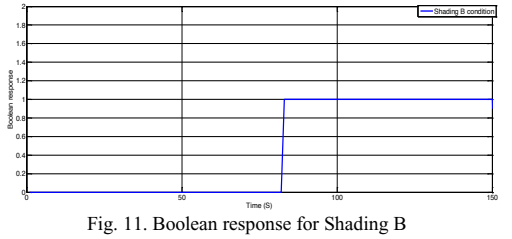

Fig. 11. Boolean response for Shading B

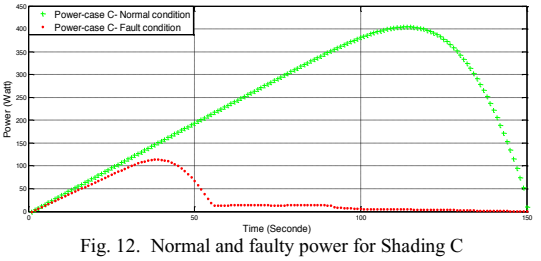

Fig. 12. Normal and faulty power for Shading C

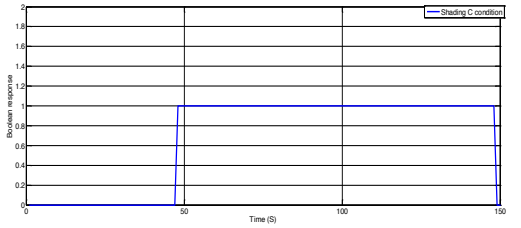

Fig. 13. Boolean response for Shading C

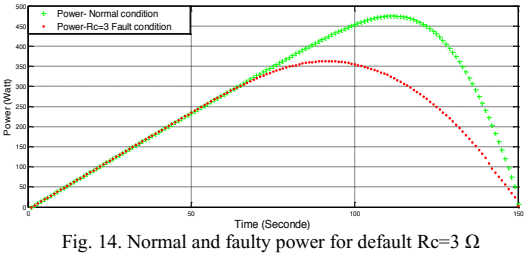

Fig. 14. Normal and faulty power for default Rc=3 Ω

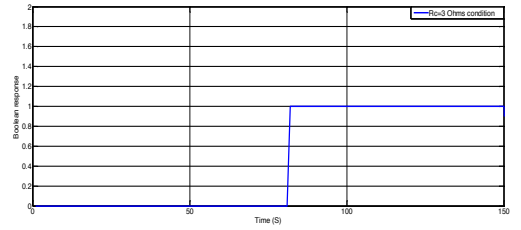

Fig. 15. Boolean response for default Rc=3Ω.

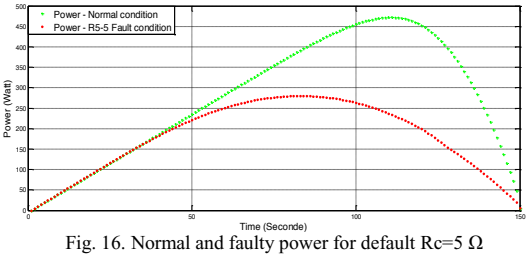

Fig. 16. Normal and faulty power for default Rc=5 Ω

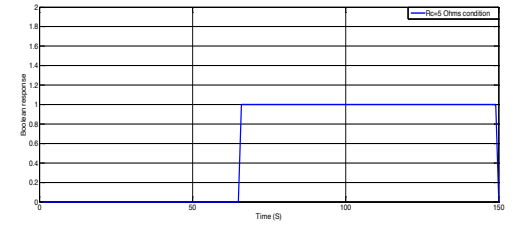

Fig. 17. Boolean response for default Rc=5Ω

4. Conclusion

The diagnosis method presented here is built on an accurate two diodes model of a photovoltaic module and it allows to calculate the characteristic threshold of normality and threshold of failure in five cases. The electrical signature of the considered five faults is established from the observed deformations on their associated curves and validated by numerous field tests. These deformations change the three major points and the slopes of the three associated parameters for each curves. The fault detection is made by comparing an ideal estimated power with measured performance. The recognition of the occurrence of a fault is made using the threshold method of the residual signals.

This diagnosis method previously used, is suitable for electrical signatures of selected faults located on Simscape based model of a photovoltaic panel. Fault detection and identification are properly performed by this approach for each evaluated case. However, the detection time depends on the speed of the flash test. Further, the distinction between electrical signatures of different faults can be distorted by noise. This could show the interest of an efficient anti-noise processing (e.g. Wald test...). Globally, this diagnosis approach allows a good detection for the considered faults.

References

[1] Alers GB. Solar photovoltaic module failure analysis. Microelectronics Failure Analysis: Desk Reference, 2011.

[2] Kazmerski LL. Photovoltaics characterization: A survey of diagnostic measurements. Journal of materials research. 1998 Oct 1;13(10):2684-708.

[3] Chouder A, Silvestre S. Automatic supervision and fault detection of PV systems based on power losses analysis. Energy Conversion and Management. 2010 Oct 31;51(10):1929-37.

[4] Riley D, Johnson J. Photovoltaic prognostics and heath management using learning algorithms. In Photovoltaic Specialists Conference (PVSC), 2012 38th IEEE 2012 Jun 3 (pp. 001535-001539). IEEE.

[5] Skoplaki E, Palyvos JA. On the temperature dependence of photovoltaic module electrical performance: A review of efficiency/power correlations. Solar energy. 2009 May 31;83(5):614-24.

[6] Ishaque K, Salam Z, Taheri H. Simple, fast and accurate two-diode model for photovoltaic modules. Solar Energy Materials and Solar Cells. 2011 Feb 28;95(2):586-94.

[7] Davarifar M, Rabhi A, El Hajjaji A, Dahmane M. New method for fault detection of PV panels in domestic applications. In3rd International Conference on Systems and Control 2013 Oct 29 (pp. 727-732). IEEE.

[8] Bouraiou A, Hamouda M, Chaker A, Sadok M, Mostefaoui M, Lachtar S. Modeling and simulation of photovoltaic module and array based on one and two diode model using Matlab/Simulink. Energy Procedia. 2015 Aug 31;74:864-77.

[9] CHINALIGHT SOLAR; 2003. Available from: http://www.chinalightsolar.com/en.

[10] Poli R, Kennedy J, Blackwell T. Particle swarm optimization. Swarm intelligence. 2007 Jun 1;1(1):33-57.

[11] Couceiro MS, Rocha RP, Ferreira NF, Machado JT. Introducing the fractional-order Darwinian PSO. Signal, Image and Video Processing. 2012 Sep 1;6(3):343-50.

[12] Davarifar M, Rabhi A, El-Hajjaji A. Modeling of Solar Photovoltaic Panels in Matlab/Simscape Environment. In International Conference on Renewable Energy: Generation and Applications, ICREGA 2012 Jun 20 (Vol. 12).

[13] Ducange P, Fazzolari M, Lazzerini B, Marcelloni F. An intelligent system for detecting faults in photovoltaic fields. In Intelligent systems design and applications (ISDA), 2011 11th international conference on 2011 Nov 22 (pp. 1341-1346). IEEE.

[14] Firth SK, Lomas KJ, Rees SJ. A simple model of PV system performance and its use in fault detection. Solar Energy. 2010 Apr 30;84(4):624-35.

[15] Tina GM, Grasso AD, Gagliano A. Monitoring of solar cogenerative PVT power plants: Overview and a practical example. Sustainable Energy Technologies and Assessments. 2015 Jun 30;10:90-101.

[16] Evans DL. Simplified method for predicting photovoltaic array output. Solar energy. 1981 Jan 1;27(6):555-60.

[17] Patel H, Agarwal V. MATLAB-based modeling to study the effects of partial shading on PV array characteristics. IEEE transactions on energy conversion. 2008 Mar;23(1):302-10.

[18] Spataru S, Sera D, Kerekes T, Teodorescu R. Diagnostic method for photovoltaic systems based on light I–V measurements. Solar Energy. 2015 Sep 30;119:29-44.